Czech technical university
Faculty of Nuclear Sciences and Physical Engineering
Department of Physics

Bachelor Thesis

Quark-gluon plasma and study of its properties in ALICE experiment at LHC

Michal Petráň

Supervisor: RNDr.Vojtěch Petráček, CSc. Prague, June 7, 2006

Contents

Abstract

Název práce:
Vlastnosti kvark-gluonového plazmatu a možnosti jeho studia v experimentu ALICE na urychlovači LHC

Autor: Michal Petráň

Obor: Jaderné inženýrství

Druh práce: Bakalářská práce

Vedoucí práce: RNDr. Vojtěch Petráček, CSc. Katedra fyziky, Fakulta jaderná a fyzikálně inženýrská, České vysoké učení technické v Praze

Konzultant: —

Abstrakt: Současné experimenty v oblasti ultra-relativistických srážek těžkých iontů poukazují na možnost, že v nich můžeme simulovat podmínky, za jakých existovala hmota několik mikrosekund po Velkém Třesku. Ukazuje se, že se hmota nacházela v dosud neznámé, tzv. dekonfinované, fázi, kdy kvarky a gluony koexistují nevázaně. Dochází k tomu za velmi vysokých teplot a hustot. V současné době se připravuje experiment ALICE na urychlovači LHC v CERNu, který poskytne opět hlubší sondu do struktury hmoty.

Klíčová slova: Kvark-gluonové plazma, Srážky těžkých iontů, ALICE.

Title:
Quark-gluon plasma and study of its properties in ALICE experiment at LHC

Author: Michal Petráň

Abstract: Present experiments in the ultra-relativistic heavy-ion collision area are showing a possibility to simulate similar conditions as they were a few microseconds after the Big Bang. They revealed that the matter had existed in totally new, so called deconfined, phase, where quarks and gluons coexist together unbound. It happens at very high temperatures and densities. Currently there is an experiment called ALICE being prepared at LHC CERN, which will grant us deeper probe to the structure of matter.

Key words: Quark-gluon plasma, Heavy-ion collisions, ALICE.

Prohlášení

Prohlašuji, že jsem svou bakalářskou práci vypracoval samostatně a použil jsem pouze podklady a zdroje (literatury, projekty, SW, atd.) uvedené v přiloženém seznamu.

Nemám žádný důvod proti užití tohoto školního díla ve smyslu §60 Zákona č. 121/2000 Sb., o právu autorském, o právech souvisejících s právem autorským a o změně některých zákonů (autroský zákon).

V Praze dne:

Acknowledgement

First of all, I would like to thank my supervisor Vojtěch Petráček for his invaluable help, motivation and guidance through the preparation of this thesis. Last but not least I would like to thank him for the much needed language corrections.

I also express my gratitude to others from Dept. of Physics at Faculty of Nuclear Sciences and Physical Engineering, CTU for their occasional advice in different topics.

Finally, I am grateful to my parents and to Lucka for their patience and support.

1 Physics overview

1.1 Elementary particles

According to nowadays observations and theories, we distinguish two big groups of elementary particles from which all the matter, as we know it, is made of. These two groups are **leptons** and **quarks**. Both are fermions. Besides those, we also know particles which are exchanged in interactions and these are bosons.

1.1.1 Leptons

Leptons are relatively light particles. We know six leptons divided into three generations, electron with electron neutrino, muon with muon neutrino and the heaviest tauon (or tau lepton) with tau neutrino.

$$\begin{pmatrix} e \\ \nu_e \end{pmatrix} \begin{pmatrix} \mu \\ \nu_\mu \end{pmatrix} \begin{pmatrix} \tau \\ \nu_\tau \end{pmatrix}$$

With their anti-particles, these are the 12 leptons we have. For the reason of conservation laws (see section 1.2) we assign new property called *lepton number* to each of them. After each generation, we have electron number L_e, muon number L_μ and tau number L_τ. Lepton classification is summarized in table 1.1.

Table 1.1: Lepton classification

	l	Q	L_e	L_μ	L_τ
First generation	e	-1	1	0	0
	ν_e	0	1	0	0
Second generation	μ	-1	0	1	0
	ν_μ	0	0	1	0
Third generation	τ	-1	0	0	1
	ν_τ	0	0	0	1

1.1.2 Quarks and Hadrons

Unlike the leptons, heavier particles, such as nucleons, are composed of smaller constituents, which we call quarks. Three generations of quarks have been discovered. The first generation *up* and *down*, second generation *strange* and *charm* and third generation *bottom* and *top* quark (sometimes we can find them it the literature as *beauty* and *truth*).

$$\begin{pmatrix} d \\ u \end{pmatrix} \begin{pmatrix} s \\ c \end{pmatrix} \begin{pmatrix} b \\ t \end{pmatrix}$$

Quarks have completely new degree of freedom called *color* with three different states; *red, green, blue* (and their anti-colors). They don't exist separately, they form bound colorless (in analogy to optical composition of colors) states of two or three quarks. These combinations are called *hadrons*, a pair of quark and antiquark is called *meson* and a triplet is a *baryon*. The six quarks can be

Table 1.2: Quark classification

	q	Q	S	C	B	T
First generation	d	$-\frac{1}{3}$	0	0	0	0
	u	$\frac{2}{3}$	0	0	0	0
Second generation	s	$-\frac{1}{3}$	-1	0	0	0
	c	$\frac{2}{3}$	0	1	0	0
Third generation	b	$-\frac{1}{3}$	0	0	-1	0
	t	$\frac{2}{3}$	0	0	0	1

found creating various combinations (in theory all six, but experimentally the top quark does not form any bound states because it simply decays before it can even interact with another particle).

Until 1974 only first three quarks were known. In 1974 the c quark has been experimentally confirmed and new combinations were observed. Three years later the b quark was observed. Since then, the scientists waited a long time to find a partner of the b quark and finally in 1995 the t quark has been discovered. The quarks are characterized by their electric charge(Q), strangeness(S), charm(C), beauty(B) and truth(T). Quarks' properties are summarized in table 1.2. (We don't include upness(U) and downness(D), because they are redundant. For instance the only quark with $S = C = B = T = 0$ and charge $Q = \frac{2}{3}$ is the u quark.)

1.2 Basic Interactions

1.2.1 Four forces

As far as we know, there are just four fundamental forces in nature: *strong, electromagnetic, weak,* and *gravitational*. Everyone of these is described by a physical theory and exchange of a virtual particle (boson) called mediator (for gravity yet hypothetical). Their strength and mass of the mediator varies for each interaction (see table 1.3).

Table 1.3: Interaction classification

Force	Strength	Theory
Strong	10	Chromodynamics
Electromagnetic	10^{-2}	Electrodynamics
Weak	10^{-13}	Flavordynamics
Gravitational	10^{-42}	Geometrodynamics

Force	Mediator	Mediator mass
Strong	Gluon	~ 0
Electromagnetic	Photon	0
Weak	W and Z	82 and 92 GeV
Gravitational	Graviton	?

As we see from the magnitude, we can neglect the gravitational interaction as it has insignificant influence on reactions at timescales of our concern. Now we will discuss the properties of strong, weak and electromagnetic interactions in particle reactions.

1.2.2 Conservation laws

For better illustration how to understand different interactions, let us draw the Feynmann's diagram of each (figure 1). Two particles cannot interact however

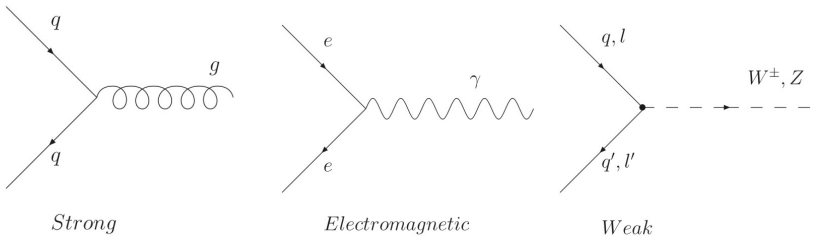

Figure 1: Vertices of three basic interactions, incoming and outgoing particles on the left and the mediator on the right. q, q' stands for quarks, e, l, l' stands for leptons, γ, g, $W^{\pm}$, Z stands for photon, gluon and intermediate vector bosons respectively

they like, it is observed that they are limited by some conservation laws. Let's go through them one by one.

1. Conservation of charge : All three interactions conserve electric charge. In case of the weak interaction the charge can be carried in or out of a vertex by charged mediator, but is conserved in every vertex.

2. Conservation of color : The weak and electromagnetic interaction does not affect color. Similarly to weak interaction and the charge, in strong vertex, the color of interacting particle can be changed by its mediator, the gluon. But again, in each vertex it is conserved.

3. Conservation of baryon number : At each vertex, the number of incoming quarks equals the number of those which are outgoing. As quarks can't come to a reaction alone, they always come in baryons (with quark number 3), antibaryons (quark number -3), or mesons composed of a quark and antiquark (quark number +1-1=0), so it is more convenient to speak of the baryon number more then quark number, which is +1 for baryon and -1 for anti-baryon. Technically speaking, it is 1/3 of the quark number.

4. Conservation of electron, muon and tau number : The strong force do not touch leptons at all, in the electromagnetic interaction the same particle that goes in, comes out of the reaction. The weak interaction only mix together leptons from the same generation. (We could invent similar thing for the quarks, such as conservation of generation of quarks, but as the weak interaction can actually change the generation of quark in an interaction, we have another reason to use the baryon number mentioned above).

There is a few more rules for prediction of possible decays and reactions, but as they are not absolute (as those above), they speak only of probability of a reaction, I will not mention them here. They can be found for example in [1].

2 Quark-gluon plasma

2.1 Big Bang

What was the Universe like before $10\mu s$ after the Big Bang? Relatively small volume was occupied by very dense and very hot matter. Then the Universe expanded and cooled until today state. Our aim is to simulate that very dense hot matter in a laboratory. We accelerate particles to high velocities and let them collide with each other. There are (for a short period of time) similar conditions as in the early Universe. Of course the time and baryon density scales are rather different in our "micro bang". But we should be able to see the dissolution of hadrons to quarks at energy densities exceeding 1 GeV fm^{-3}. We can approach this state from two directions. We can increase the temperature at constant baryon density, or the other way around. Different experiments followed different paths as marked in figure (2).

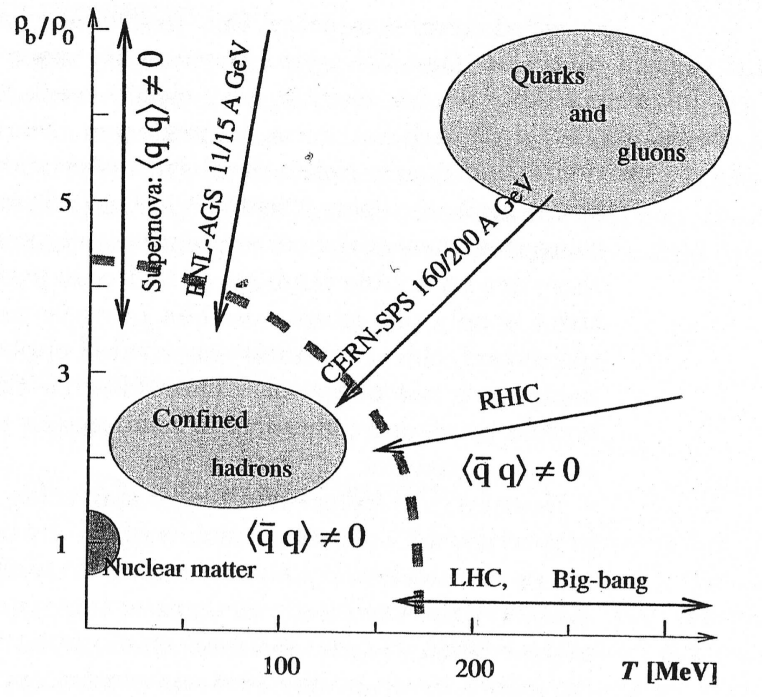

Figure 2: Different approaches to QGP state of a few experiments. It shows the path of relatively cold neutrons stars turning into supernovas, which has high relative baryon density ρ_b/ρ_0 and the opposite, Big Bang following the path of relatively low baryon density, but very high temperature T.

Well spatially localized drop containing the energy of two colliding particles, this small fireball of very hot matter, will not be stable at all, it will actually explode very fast ($t \simeq 10^{-23}$ s). After the expansion of the fireball, we observe numerous newly created hadronic particles with relatively low energies instead of a few high-energetic particles as we would in elastic scattering. We study the conversion of kinetic energy brought to the system by colliding particles to

completely new particles at high multiplicities and lower energies. This evolution of the fireball is thought to be very similar (despite the fact that it is much faster and smaller) to the one at the early stage of the Universe. Heavy-ion collisions gives us means to study the deconfined state of quarks and gluons which we call quark-gluon plasma (QGP).

2.2 Strangeness

One of the arguments supporting the deconfinement of quarks and gluons is the production of strangeness. When we make collide two nuclei (containing only u and d quarks), we observe newly created particles containing one or more strange quarks, "strange" particles (e.g. $\Xi, \bar{\Omega}, \ldots$)(see figure 3). The $s\bar{s}$ pairs are created mainly in gluon-gluon collision in the dense matter of the fireball and during the hadronization phase (see section 2.4 and 2.5) they form bound states (particles) with each other ($\bar{\Omega}(\bar{s}\bar{s}\bar{s})$) and/or u and d quarks ($\Xi(ssu)$) present in the fireball. Strange particles are naturally radioactive and decay by weak interaction (the only interaction, which can change the generation of quark). This happens on a time scale extremely long in respect to timescales of nuclear collisions and strong interactions. It is very convenient, as the detection of strange particles is made relatively easy by examining their decay products. Strangeness created

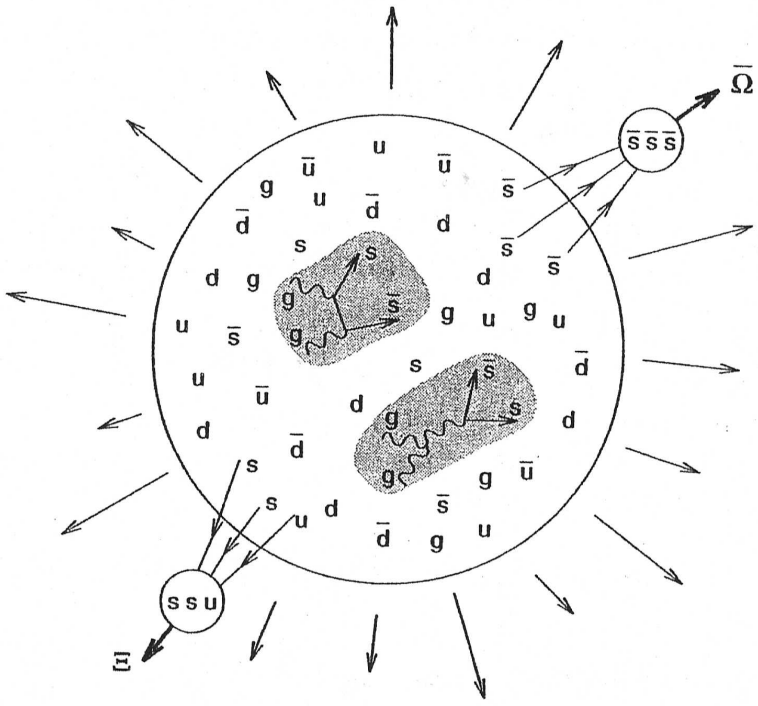

Figure 3: Possible creation of strangeness in nuclear collision

in a collision is proportional to kinetic energy of colliding particles. We find that there is a threshold for strangeness production, obviously proportional to 2 masses of strange quark, and fast increase of strange particles production observed in the region of energies 5 GeV $\leq \sqrt{s} \leq$ 17 GeV [2] (see the next

section for definition of $\sqrt{s}$) . But at higher energies, production of strange particles is restricted by melting of $s\bar{s}$ pairs in the fireball and production of heavier $c\bar{c}$ (or even $b\bar{b}$) quark pairs.

2.3 Describing a collision

2.3.1 Geometry and available energy

We expect the geometry to be very important in nuclear collisions. It will certainly determine the amount of particles participating in the collision. It is proven that the reaction radius defined as the square root of the reaction cross section σ rises linearly with the geometric size of the colliding nuclei;

$$\sqrt{\sigma} \propto (R_p + R_t) \propto (A_p^{1/3} + A_t^{1/3}), \tag{1}$$

where subscripts p and t stands for projectile and target nucleus respectively, A is the nucleus atomic number, R is the nucleus radius. As we see from the

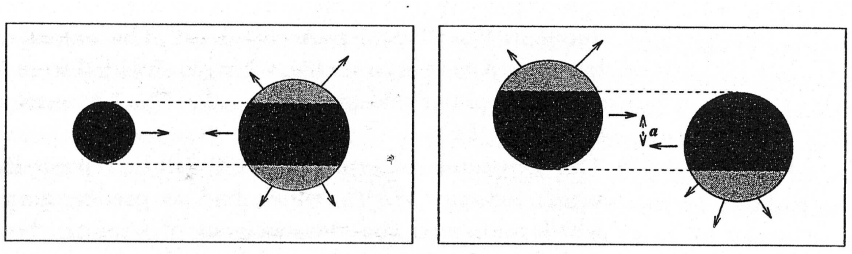

Figure 4: Left: asymmetric, but central collision of two different nuclei. Right: symmetric decentralized collision of two nuclei of the same nature with impact parameter a. In both cases black parts are involved in the reaction, grey parts play roles of "spectator" matter. Arrows show the direction in which products will be emitted.

figure (4), reaction geometry is necessary to minimize the amount of spectator matter, which can pollute the experimental data.
We mentioned a few times energy of the collision in the above text. During an interaction, the energy must be conserved, summarized energy of all the products must be the same as the energy of the two colliding nuclei. As the colliding particles are usually relativistic, we have to introduce a Lorenz invariant quantity to describe the reaction. It terms of energies and momenta of the projectile (p) and the target (t) it is

$$\sqrt{s_{pt}} \equiv \sqrt{(E_p + E_t)^2 - (\vec{p}_p + \vec{p}_t)^2}. \tag{2}$$

In the CM frame the sum $\vec{p}_p + \vec{p}_t = 0$ by definition and the $\sqrt{s_{pt}}$ is recognized as the available reaction energy. As it is an invariant of the Lorenz transformation, we can evaluate it in any frame of reference. It can be generalized to n-body collision, but it is very difficult to collide more than two bodies at the same time. On the other hand, we can use this (defined by equation (3)) generalization to

determine $\sqrt{s^{(n)}}$ of the many-body products of a reaction

$$\sqrt{s^{(n)}} \equiv \sqrt{\left(\sum_{i=1}^{n} E_i\right)^2 - \left(\sum_{i=1}^{n} \vec{p}_i\right)^2}, \tag{3}$$

which has to be equal to the reaction energy $\sqrt{s_{pt}}$. We actually talk about the *invariant mass* of the system.

2.3.2 Rapidity and Pseudorapidity

For description of the collision dynamics we introduce new variable called rapidity. At first, let us have a look at the particle momenta in the collision. We can decompose those into a longitudinal component ($\vec{p}_L$) along the collision axis and a transverse component ($\vec{p}_\perp$) perpendicular to the collision axis. Longitudinal

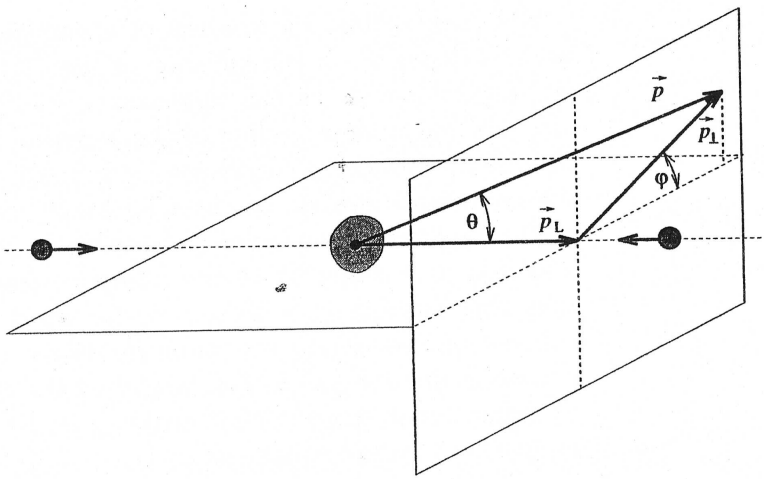

Figure 5: Particle momentum $\vec{p}$ decomposition in the CM frame into $\vec{p_L}$, $\vec{p_\perp}$ characterized by the inclination angle θ and azimuthal angle φ.

momentum is an inconvenient variable since it depends of the CM (center of mass) frame velocity in reference to the laboratory frame. For analysis we have to transform the coordinate system to CM frame of reference. This will be much easier replacing p_L by *rapidity* y, because y is additive under successive Lorenz transformations along the same direction. It is defined as follows:

$$E = m_\perp \cosh y, \qquad p_L = m_\perp \sinh y, \tag{4}$$

where $m_\perp$ is the transverse mass:

$$m_\perp = \sqrt{m^2 + \vec{p}_\perp{}^2}. \tag{5}$$

For the velocity v_L of the particle, we have the relation from equation (4)

$$v_L \equiv \frac{cp}{E} = c \tanh y. \tag{6}$$

When we want to express the rapidity y, we get

$$y = \frac{1}{2}\ln\left(\frac{1+v_L}{1-v_L}\right) = \frac{1}{2}\ln\left(\frac{E+p_L}{E-p_L}\right) = \frac{1}{2}\ln\left(\frac{E+p_L}{m_\perp}\right) \tag{7}$$

Now we will verify the simplicity of Lorenz transformation along the collision axis. Under such transformation $m_\perp$ and $\vec{p}_\perp$ stay unchanged, energy and longitudinal component of momentum transform as:

$$E' = \gamma_c(E + v_c p_L) \qquad p'_L = \gamma_c(p_L + v_c E). \tag{8}$$

Primed variables are seen in the laboratory system, which moves with velocity v_c with respect to the CM frame of reference, in which the other quantities (E, p_L) are measured. The factor γ_c is the Lorenz contraction factor. The rapidity of the transformation y_c then can be written as:

$$\cosh y_c = \gamma_c, \qquad \sinh y_c = \gamma_c v_c. \tag{9}$$

Using the equation (4) and (9) we find

$$E' = m_\perp \cosh(y + y_c) \qquad p'_L = m_\perp \sinh(y + y_c). \tag{10}$$

From equation (10) is evident, that the rapidity in the laboratory system y' is in terms of the CM frame rapidity y and rapidity of the transformation y_c

$$y' = y + y_c \tag{11}$$

Trivial application of this is the rapidity in symmetric collider experiments, where laboratory and CM systems are the same. We will appreciate the use of rapidity in asymmetric (different nuclei) collisions or fixed target experiments where the CM is moving in respect to laboratory system.
In the experiments, observed particles are often not identified yet, so we don't know their masses, which are required to determine the particle's rapidity. What we usually know is the particle momentum measured by deflection within a magnetic field. In most experiments, the particle momentum is much greater then the particle mass. Let us see what happens with rapidity using the approximation

$$E = \sqrt{p^2 + m^2} \longrightarrow p \qquad m_\perp = \sqrt{m^2 + \vec{p}_\perp{}^2} \longrightarrow p_\perp \tag{12}$$

Now we can define in analogy to equation (4) a simpler variable, the *pseudorapidity* η:

$$p = p_\perp \cosh\eta, \qquad p_L = p_\perp \sinh\eta \tag{13}$$

As in equation (7) we can express pseudorapidity η (also see figure (5) for θ definition)

$$\eta = \frac{1}{2}\ln\left(\frac{p+p_L}{p-p_L}\right) = \frac{1}{2}\ln\left(\frac{1+\cos\theta}{1-\cos\theta}\right) = \ln\left(\cot\frac{\theta}{2}\right) = -\ln\left(\tan\frac{\theta}{2}\right) \tag{14}$$

This gives us the possibility to determine pseudorapidity knowing only particle-emission angle from the beam axis θ and vice versa, measuring particle-emission angle gives us (using the relation (14)) information about particle pseudorapidity. We can use pseudorapidity to describe azimuthal coverage of a detector (see also section(4.2)). For example at LHC, the rapidity coverage region is about $\eta \simeq 8.5$, which corresponds to $\theta = \pm 4.5 \times 10^{-4}$ rad ($\equiv 0.025°$). From equations (4) and (13) one can obtain implicit relations between pseudorapidity and rapidity:

$$m_\perp \sinh y = p_\perp \sinh\eta, \qquad E\tanh y = p\tanh\eta. \tag{15}$$

2.4 Evolution of the fireball

Let us have a closer look at what happens with the fireball right after a collision. We can expect that an equilibrium is being established. If we search for a position-dependent parameter to characterize equilibration, we find the average energy per particle, which is in other words temperature T. But only temperature is not sufficient to describe a system where different particles are present. We have to introduce chemical potential μ_i for each of i types of particles in the fireball. This will give us the mean to regulate particle (quark-flavor) density.
Thermal equilibration is the state of matter, where the energy is equally distributed among all particles present in the fireball. This leads to statistical distribution of energy, which can be achieved only by elastic scattering. We can use temperature T to describe the state of the fireball only if thermal equilibrium has been (almost) reached. We will call the time at which this happens τ_{th}.
Chemical equilibration takes more time. Reactions changing particles into another are necessary to take place in order to make chemical potentials μ_i equally strong. This would be the *relative* chemical equilibrium. Let us call the relevant time scale τ^{rel}_{chem}.
Absolute chemical equilibrium is achieved when we take into account energy-matter conversion. We expect to approach this more slowly than the relative equilibrium. Again, we will call the relative time scale τ^{abs}_{chem}. For the absolute chemical equilibrium, we introduce the *fugacity factor* γ_i for each particle. Then we can write the chemical potential of particle i and it's antiparticle as:

$$\mu_i^{\pm} = \pm\mu_i + T\ln\gamma_i$$

Then we study the evolution of fugacity factor, which should approach $\gamma_i = 1$. So we have a relation between the relaxation times:

$$10^{-22}\text{ s} > \tau^{exp} \simeq \tau^{abs}_{chem} \geq \tau^{rel}_{chem} > \tau_{th},$$

where τ^{exp} is the time light needs to traverse the largest nuclei participating in the collision.

Now we can summarize how the fireball evolves starting from the collision ending by "freeze-out" and hadronization. We will present experimental observations of the time scales. For an illustration see Figure 6.

1. Initial quantum stage.
   Here the formation of the fireball itself takes place. It happens in times $0 \leq t \leq \tau_{th}$. This phase is very difficult to study and describe in terms of quantum mechanics. Times varies from 0.25 to 1 fm/c depending on the particle density and temperature in the collision.

2. The subsequent chemical equilibration.
   This stage lasts for at least ~ 1.5 fm/c (in some conditions it can be even faster, around 0.6 fm/c). Particle production reactions take place during this time and chemical equilibration of the light quarks u, d is established. Temperature falls rapidly.

3. The strangeness chemical equilibration.
   Third period lasting up to ~ 5 fm/c, in which production and chemical

equilibration of the strange quark is observed. Temperature falls mainly because of the fireball expansion.

4. The hadronization / freeze-out.
   Fireball of dense matter expands to dimensions, which do not allow any further chemical re-equilibration of the final state particles.

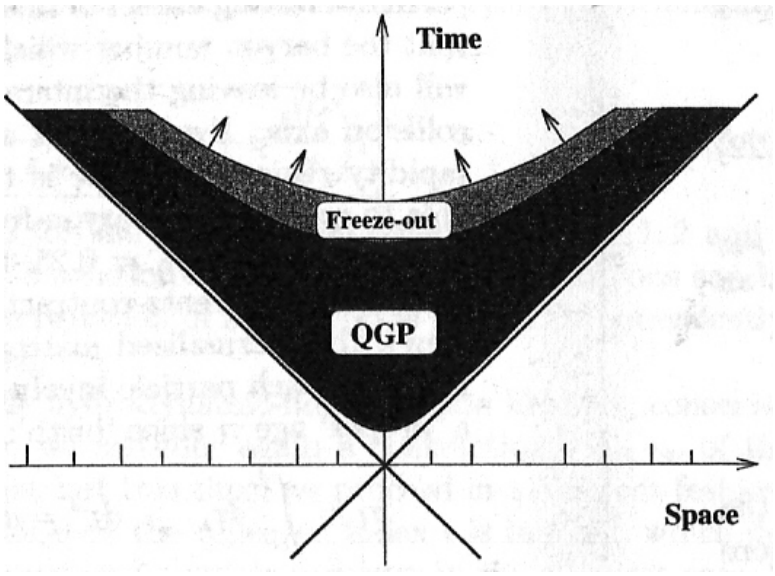

Figure 6: Evolution of a heavy-ion collision seen in space-time coordinates. The light cone represent the causality limit for the energy flow.

Then, we observe the final state particles, their number and properties (momentum, rapidity,...) and try to reconstruct the whole event.

2.5 Phase transition

At relativistic energies, we expect the matter and structured confined vacuum to dissolve, forming a domain of thermally equilibrated hadronic matter of freely movable quarks and gluons. For high temperature T and/or high relative baryon density ρ_b/ρ_0 (see figure (2) the deconfined phase is attained. During an experiment, when the deconfinement is reached, it freezes back to confined state as hadronic gas (HG) as described in section 2.4. When exactly the phase transition occurs is determined by Gibbs' equilibrium conditions. In this state of matter, small clusters of hadronic matter exist in hot bath of deconfined quarks and gluons.
First condition is pressure equilibrium (we use index 1 for QGP and 2 for HG):

$$P_1 = P_2.$$

This will assure the absence of any force to the phase boundary. Second condition is equilibration of temperature

$$T_1 = T_2,$$

which (in correspondence with the 0. law of thermodynamics) will eliminate all radiation transport of energy between the two phases. In figure (7) we see three

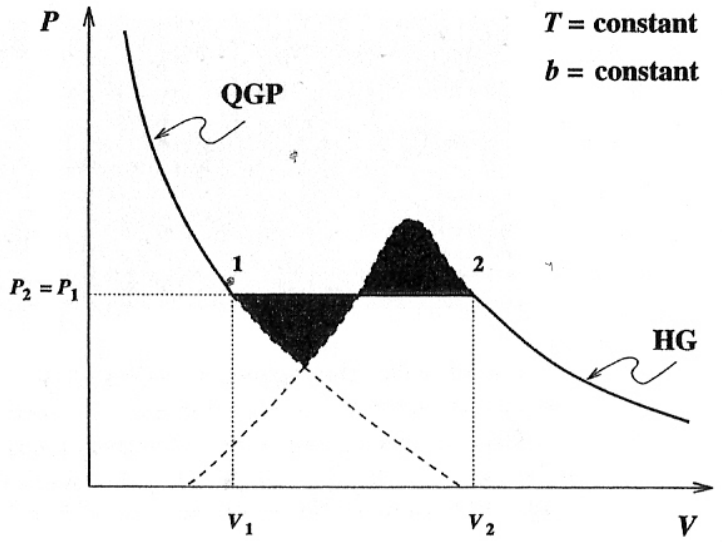

Figure 7: The p-V diagram of QGP-HG phase transition at fixed temperature T and baryon number b. Dashed lines indicate unstable domains of overheated and undercooled phases and black regions indicate areas of possible values of p and V during the phase transition.

domains;

1. The HG region for $V > V_2$.
2. The QGP region for $V < V_1$, where hadrons totally disappear.
3. The Van der Waals region for $V_1 < V < V_2$. In this region small clusters of confined quarks (hadron-like matter) begin to appear at V_1 in the QGP phase. From the other side, at V_2 small drops of deconfined quarks and gluons are created in the HG, individual hadrons are dissolved into QGP clusters.

In order to determine the critical pressure $P_1 = P_2 = P_{12}$, we require the work done along the transition to vanish, it means

$$\int_{V_1}^{V_2} (P - P_{12}) dV = 0$$

(black shaded area in figure 7). For the third Gibbs condition, we have to introduce baryochemical potential μ and we require

$$\mu_1 = \mu_2$$

along the phase boundary. During the phase transition, we observe discontinuity in energy density, entropy density and baryon density across the phase boundary.

Now we will search for the magnitude of the temperature at which the deconfined phase of quarks and gluons will freeze into hadrons. Using relation (generalized Stefan-Boltzmann law, [2])

$$P_c = \frac{1}{3}\epsilon_c = \frac{\pi^2}{90} g T_c^4, \tag{16}$$

where subscript c means the critical values at the phase transition. The factor

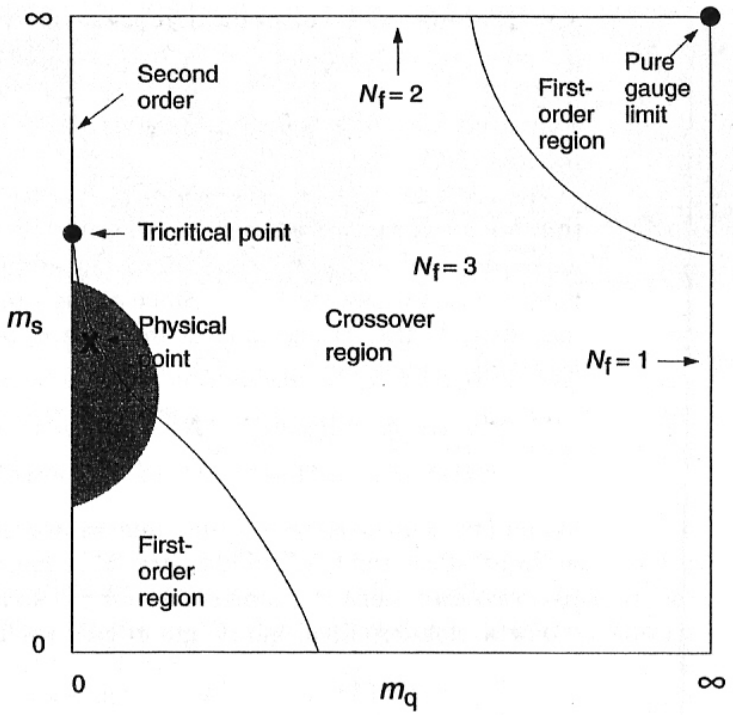

Figure 8: Varying nature of phase transition at finite temperature as a function of quark masses m_q and m_s.

g is the degeneracy factor which is technically number of degrees of freedom available. In the deconfined phase we have

$$g \equiv g_g + \frac{7}{4} g_q,$$

where g_g is the contribution from gluons (bosons) and g_q is the one from quarks (fermions). The factor $\frac{7}{4} = 2 \times \frac{7}{8}$ comprises the factor 2 for particle-antiparticle multiplicity and the factor $\frac{7}{8}$ for smaller fermion phase space relatively to the boson one (fermions obey the Pauli's exclusion principle). Recalling spin and color for both quarks and gluons and flavor for quarks, we obtain the following degeneracy in the deconfined phase:

$$\begin{aligned} \text{gluons} : g_g &= 2(\text{spin}) \times (N_c^2 - 1)(\text{color}) = 2 \times 8 = 16 \\ \text{quarks} : g_q &= 2(\text{spin}) \times N_c(\text{color}) \times n_f(\text{flavor}) = 2 \times 3 \times n_f \end{aligned}$$

The g_q depends on how many flavors we will take into account. For the two light quarks u, d, it is equal to 2. But at high temperature we may have to include the s quark. For our evaluation, we can approximate n_f by effective value of flavors $n_f = 2.5$. (At even higher temperature, the factor n_f would rise of course as the we would reach the mass of heavier (c, b, t) quarks.) We get for g:

$$g = g_g + \frac{7}{4} g_q = 16 + \frac{7}{4} \times 6 \times 2.5 = 16 + 26.25 = 42.25$$

Instating this to equation (16), and recalling the critical value of $\epsilon_c \simeq 1 \text{ GeV} \cdot \text{fm}^{-3}$ from section 2.1, we get the value

$$T_c \simeq 160\text{MeV}.$$

This value was confirmed by numerical simulations of QCD [†] at zero baryon density, but if we introduce (non zero) quark masses $m_q \equiv m_u = m_d$ and m_s, we observe rapid changes in this value. Then, various phase properties emerge as well as the phase transition order (see figure (8)). This temperature represents the critical point at which the phase transition takes place. After the hadronization, the newly created particles still affect each other. The fireball expands and cools down and at the temperature of $T \simeq 125$ MeV fragments stop to interact with each other, so temperature cannot be defined anymore. These two boundaries are visible in figure 6 as the black-gray phase transition and the gray-white hadron interaction boundary.

[†]QCD, quantum chromodynamics, is quantum field theory that describes the properties of the strong interactions between quarks and between protons and neutrons in the framework of quantum theory.

3 Experiments leading to discovery of QGP

3.1 SPS

The SPS (**S**uper **P**roton **S**ynchrotron) is the biggest fully functional particle accelerator at CERN. The CERN-SPS heavy ion research program has about 15 year-long tradition in fixed target mode with the energy range [2] up to 200 AGeV for up to $A \simeq 100$ and dropping to 158 AGeV for neutron rich projectiles such as Pb. For better image of the CERN accelerator complex see Appendix A.

3.2 CERES/NA45

3.2.1 Physical overview

CERES is a dilepton experiment at CERN SPS with fixed Au target. It was bombarded by Pb beam at 158 A GeV. Enhanced production of low mass e^+e^- pairs in collisions between heavy nuclei has been observed. These excess pairs had invariant mass approximately twice the pion mass and the enhancement absent in proton induced collisions leads us to pion annihilation $\pi\pi \rightarrow \rho \rightarrow e^+e^-$ as the additional source of lepton pairs. Two different theoretical models expect two different scenarios to happen with the ρ peak in the spectrum. One expects it to shift to lower mass, the other broadening and slight shift up. Testing these predictions was one of the CERES's objectives.

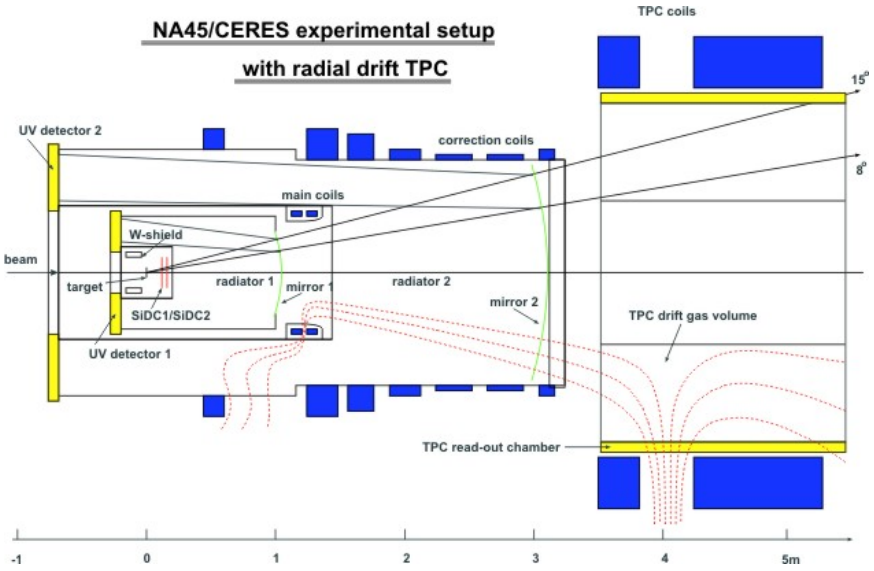

Figure 9: CERES experimental setup with TPC upgrade.

3.2.2 Experimental setup

The original setup was supplemented with a TPC in 1998, which allowed to improve the momentum resolution and particle identification capability. The upgraded experiment is shown on figure 9. Charged particles emitted from the

segmented Au target passes through two SDDs located 100mm and 138mm from the target. These two detectors are used to measure the angle of passing particle with $\Delta\theta = 0.2$ mrad and $\Delta\varphi = 0.2$ mrad resolution and determination of the primary vertex with $\Delta z = 200$ μm resolution (z coordinate is along the beam axis). Second, particle passes through two RICHes (Ring Imaging CHerenkov detector), which serve for electron identification. Unlike in the original setup, in the upgraded one the magnetic field between the two RICHes is switched off. With the two RICHes aligned, better particle identification is obtained. Finally the particles pass through the new TPC. There the ionization electrons drift outward towards the 16 readout chambers. Resolution reached with the upgraded setup was

$$\frac{\Delta p}{p} = 2\% + 1\% \text{ p/GeV}$$

About 30 million Au+Pb collisions at 158 AGeV were taken into account for the data analysis in the fall 2000. Most of the collisions happened with the centrality less then 7% of geometrical cross section.

3.3 NA49

3.3.1 Physical overview

This experiment at CERN SPS has collected large amount of experimental data on hadron production over the period of 1994-2002. It studied A-A collisions aiming at an understanding of the reaction mechanism by systematic study of many observables in different systems and at different energies. Changes of hadron production is expected once the deconfined phase is reached in the early stage of the collision. Most of the studies were performed for central Pb-Pb collisions at the top SPS energy 158 AGeV. Main observables were particle correlation and fluctuation measures, hadro-chemical composition of the final state, especially the strangeness content. For many observables the energy dependence was studied over the full SPS energy range providing almost continuous coverage.

3.3.2 Experimental setup

NA49 is a large acceptance hadron spectrometer. It is composed mainly of four large volume TPCs. Two of them are located in a magnetic field. Particle identification is done by measurement of specific energy loss in the TPCs. Centrality of the collision is determined by forward calorimeter downstream of the spectrometer. The ratio of participating and spectating nucleons is extracted by simulation based on the VENUS model.

3.4 NA50

3.4.1 Physical overview

NA50 [3] was designed to detect dimuons produced in Pb-Pb and A-p collisions at nucleon-nucleon energies $\sqrt{s} = 18$ resp. 30 GeV respectively. The physics includes direct probes of QGP, strangeness production, thermal dileptons, ϕ, J/ψ and ψ' vector mesons production. Generally speaking, it studied the charmonium suppression and strangeness enhancement in heavy ion collisions.

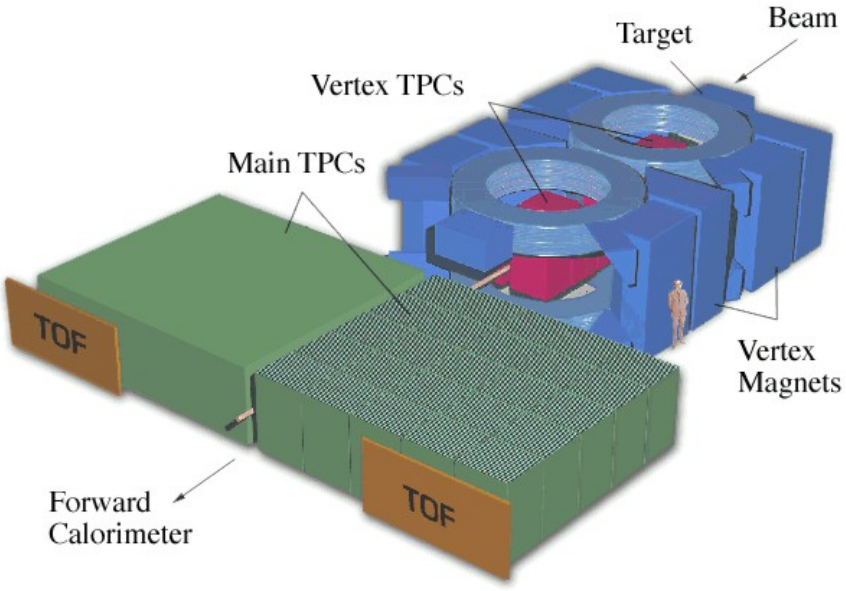

Figure 10: NA49 experimental setup.

3.4.2 Experimental setup

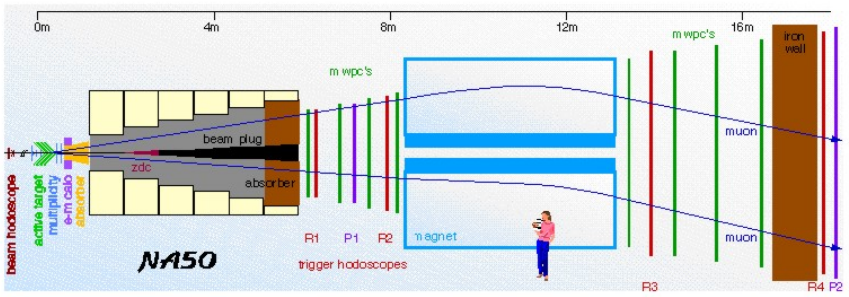

Figure 11: NA50 experimental setup.

The muons are measured in the former NA10 spectrometer, which is shielded from the target region by a beam stopper and absorber wall. The muons traverse 5 m of BeO and C. The impact parameter is determined by a Zero Degree Calorimeter (Ta with silica fibres). Energy dissipation and particle production are measured by an Electromagnetic Calorimeter (Pb and scintillating fibres) and a Multiplicity Detector (silicon strips).

3.5 NA60

3.5.1 Physical overview

The NA60 attempts detection of the charmed hadrons to complement the results of J/ψ suppression from NA50. It is an upgrade to NA50, thus it studies the same reactions, Pb-Pb and A-p collisions.

3.5.2 Experimental setup

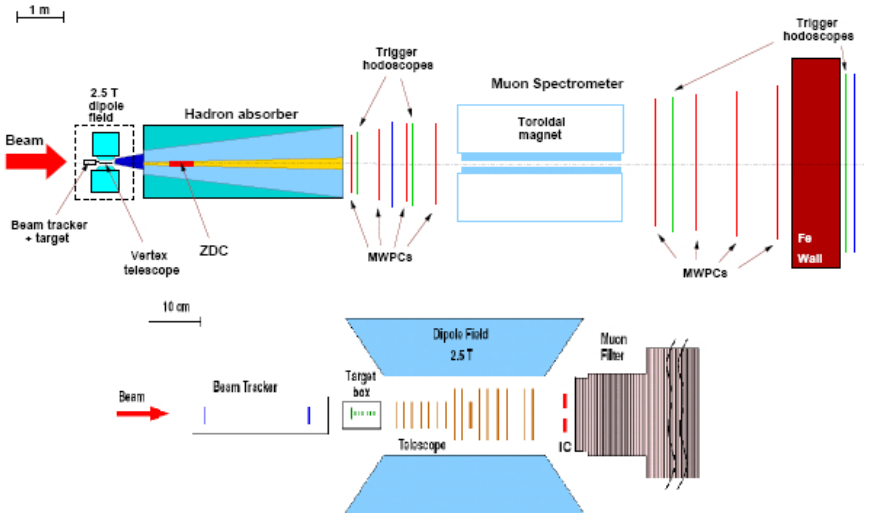

Figure 12: NA60 experimental setup.

The NA60 detector [4] complements the muon spectrometer and zero degree calorimeter previously used in NA50 with new state-of-the-art silicon detectors, placed in the target region. A radiation hard beam tracker, made of silicon microstrip detectors operated at 130 K, is placed on the beam line, upstream of the target system. It gives the transverse coordinates of the interaction point on the targets with a precision around 20 micron, allowing us to measure the offset of the muon tracks, and tag events where a pair of D mesons was produced. Downstream of the target system, and inside a dipole magnetic field of 2.5 T, we have a silicon tracking telescope, that tracks the charged particles and allows us to identify which one of them provides the best match to the muon measured in the muon spectrometer, placed behind a 5.5m silicon microstrip planes complemented by pixel planes. For the ion runs, the very high multiplicity of charged particles imposes the exclusive use of radiation tolerant pixel detectors.

3.6 NA57/WA97

3.6.1 Physical overview

NA57 is another CERN SPS experiment studying production of strange and multi-strange hadrons at mid-rapidity in heavy ion interactions as a function of

collision centrality and energy at CM [5]. It used Pb-Pb, p-Be and p-Pb collisions at 158 AGeV/c and Pb-Pb, p-Be at 40 AGeV/c. It is in fact a simple upgrade to WA97, which covers larger centrality range. Strange particles are studied via their weak decays, such as $K^0_S \longrightarrow \pi^+ + \pi^-$, $\Lambda \longrightarrow p + \pi^-$, $\Xi^- \longrightarrow \Lambda + \pi^-$ and $\Omega^- \longrightarrow \Lambda + K^-$. NA57 measured enhancement in hyperon production with following results (Pb-Pb relative to p-Be): $E(\Lambda) < E(\Xi) < E(\Omega)$ at 158 AGeV/c and $E(\Lambda) < E(\Xi)$ at 40 AGeV/c. This was theoretically predicted as a consequence of the phase transition.

3.6.2 Experimental setup

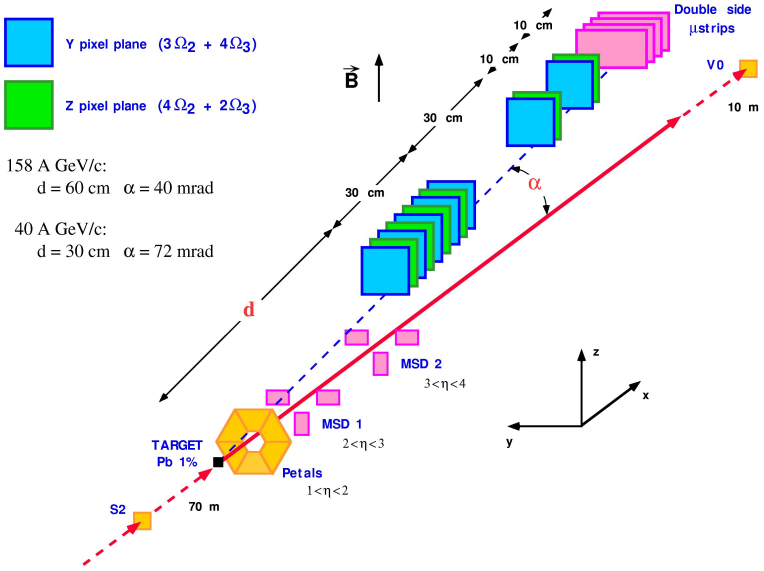

Figure 13: NA57 experiment scheme.

Tracks of the charged strange particles and their final decay products are reconstructed in $5 \times 5 \times 30$ cm^3 silicon pixel detector (see figure 13). The strange particle selection procedure uses two main criteria: (a) the two decay products must be compatible with the hypothesis of having a common origin point; (b) the reconstructed decay vertex is well separated from the target [6]. There is no direct charged particle identification, but particles are separated by kinematic cuts. Collision centrality is determined from charged particle multiplicity in pseudorapidity range $2 < \eta < 4$ by the microstrip silicon detectors, MSD (fig. 13).

3.7 WA98

3.7.1 Physical overview

WA98 is one of CERN SPS experiments developed in 1994 [7]. The main goal was to study the emission of thermal photons with high precision. These are

supposed to be the best probe of a transition from HG state to QGP, because of their weak interaction with the hot dense matter. It studied those in Pb-Pb collisions at 158 AGeV. After the collision, Plastic Ball detector measures multiplicities and momenta of fragments created in the collision. Right after Silicon Pad and Drift Chambers are used for precise determination of charged particle multiplicity. Energy flow was measured with zero-degree calorimetry. The 10000 module Lead Glass spectrometer brings high precision data on π^0 and η at midrapidity in large range of $p_\perp$ and provides photon to π^0 ratio. Photon Multiplicity Detector allows to determine the photon multiplicity in an event or event class. The charged particle setup; a Multistep Avalanche Chamber tracking system and Pad Chamber/Streamer Tube tracking system, measures momenta of charged particles produced in the collision. Time-of-Flight detectors serves as particle identification. This setup yields high statistics of transverse momentum spectra of identified hadrons as well as Bose-Einstein correlation data.

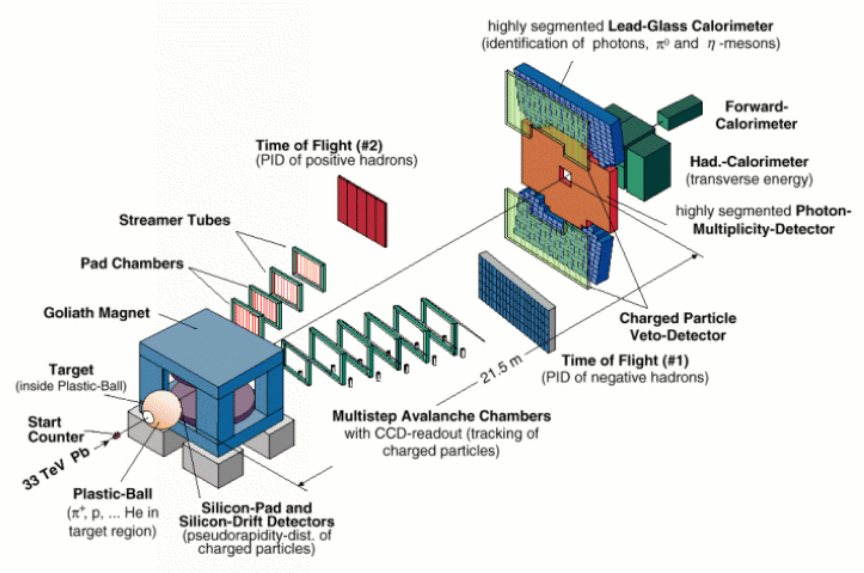

Figure 14: WA98 experimental setup.

3.7.2 Detectors

- **Plastic Ball**
  It was originally built for Bevalac at Berkley. It measures particles in the target region of polar angle $160° < q < 30°$, with full coverage of the azimuthal direction. In other words it covers almost the whole target. It consists of 655 detector modules providing particle identification using dE/E. Due to increased particle multiplicity at SPS, 160 forward modules were not used in the WA98 setup. Each dE/E module consists of two scintillators with very different timing constants. That allows to measure E with the first one and dE taking into account measurement form the second one. The signal goes through a light guide and is amplified by

a photomultiplier. Due to full azimuthal coverage, this detector is ideal for the event shape of all kinds. It is the first detector for flow (see next section for description) observation.

- **SDD - Silicon Drift Detectors**
  It is composed of circular silicon wafer of 4 inch diameter and 280 μm with 15 mm diameter hole in the middle, which allows non interacting particles to pass through. Passing charged particle creates a cloud of free electrons in the detector and they are drifted to the edge by applied voltage. Resolution of 25μm along the drift and 35μm in the azimuthal direction has been reached.

- **SPMD - Silicon Pad Multiplicity Detector**
  It is located 328mm downstream from the target. Again, it consists of circular 4 inch silicon wafer and covers a pseudorapidity range of $2.35 < \eta < 3.75$. The charge created by passing charged particle is read out directly via small pads. The wafer is divided to quadrants and each of them consists of 1012 small pads. Double hit probability is not negligible, but can be disentangled from the signal height.

- **GOLIATH Magnet**
  It is a dipole magnet with gap size from 1200 to 1600mm. Special pillars have been invented in order to optimize athe acceptance of the spectrometer. The magnet was planned to be used with two field settings; B.L=2 Tm and B.L=1 Tm.

- **MSAC - MultiStep Avalanche Chamber**
  The first tracking arm spectrometer consists of six MSACs and a Time-of-Flight (TOF). Negatively charged particles are deflected by GOLIATH to the side of the firste tracking arm. Passing through one of MSACs, charged particle ionize gas along its' path through the chamber. After an amplification, electron avalanche is produced, which excites molecules of triethylamine in the chamber to emit photons. These photons are absorbed and reemitted by wavelength shifter window and viewed by CCD camera. With hit in each of the six planes, the particle track can be reconstructed and the particle identified.

- **Pad Chambers**
  Positively charged particles are deflected by GOLIATH to the second tracking arm. It is analogous to the first tracking arm, four tracking planes are used, two Pad Chambers and two Streamer Tube detectors. The Pad Chambers are similar to the MSACs except they are read out directly. Spatial resolution of these is 1.7mm in the vertical and 0.5mm in the horizontal axis.

- **Streamer Tubes**
  They design of the Streamer Tube detectors are gas detectors with high voltage applied. It is read out via small pads. It is again supplemented by TOF for particle identification.

- **PMD - Photon Multiplicity Detector**
  Photons are detected via electromagnetic showers crated in the thick lead

plates. Newly produced particles from the shower give rise to a signal in 3 mm thick scintillator pads. These are read out by wavelength shifters coupled with CCD cameras. Hadrons will not induce any shower due to their large nuclear interaction length, but if they do, they can be easily discriminated. The PMD covers the pseudorapidity range of $2.4 < \eta < 4.4$.

- **CPV - Charged Particle Veto**
  This detector is used in conjunction with the photon spectrometer LEDA (see below) to help identify charged particles hitting the lead glass detector. It si made of streamer tubes with readout pads 4.5×1 cm. Readout chips were especially developed reaching almost 100% efficiency.

- **LEDA - LEadglass Detector Array**
  It is 10080 module leadglass calorimeter. It allows to measure photons and to reconstruct π^0 and η mesons tracks in the pseudorapidity range of 2.2 to 3. It consists of TF1 lead glass modules (cross section 4×4 cm) glued together in arrays 4×6, so-called Supermodules. Every Supermodule contains 24 photo tubes, individual high voltage generators and independent gain monitoring system. The Supermodules are stacked together forming two large subunits of approximately 5000 modules each.

- **ZDC - Zero Degree Calorimeter**
  It measures the energy of projectile spectator fragments covering the pseudorapidity range of $\eta > 5.9$ ($\sim \theta = 0.3$ around the beam axis). The ZDC is a sampling calorimeter built of 7×5 modules consisting of lead and plastic scintillators. The intensity of the scintillation light is proportional to the passing particle energy and is guided by a wavelength shifter to photomultipliers.

3.8 PHENIX

3.8.1 Overview

Pioneering **H**igh **E**nergy **N**uclear **I**nteraction e**X**periment.
[8] It is an experiment built on RHIC (Relativistic Heavy Ion Collider) at Brookhaven National Laboratory (BNL) (see appendix B). It's main purpose is to measure direct probes of high energy ion/proton collisions (such as electrons, muons and photons) and to discover and study a new state of matter, the QGP. It uses high mass resolution for observing e^+e^- pairs, which allows one to detect changes in the properties of decaying of vector mesons (e.g., $J/\psi \longrightarrow e^+e^-$, $\Phi \longrightarrow e^+e^-$).

3.8.2 Experimental setup

It comprises a central detector made of an axial field magnet and two almost identical arms placed on the left and right side of the magnet each covering ± 0.35 units of pseudorapidity. Each arm comprises several detector subsystems. The electromagnetic calorimeter lets us measure low-$p_\perp$ photons near $y = 0$. Hadrons are detected in silicon vertex detector (Pad Chambers on figure 15) for $-2.65 < \eta < 2.65$. Charged hadrons distribution is studied on event-by-event basis, but without particle identification. (More details on detector functions in [8].)

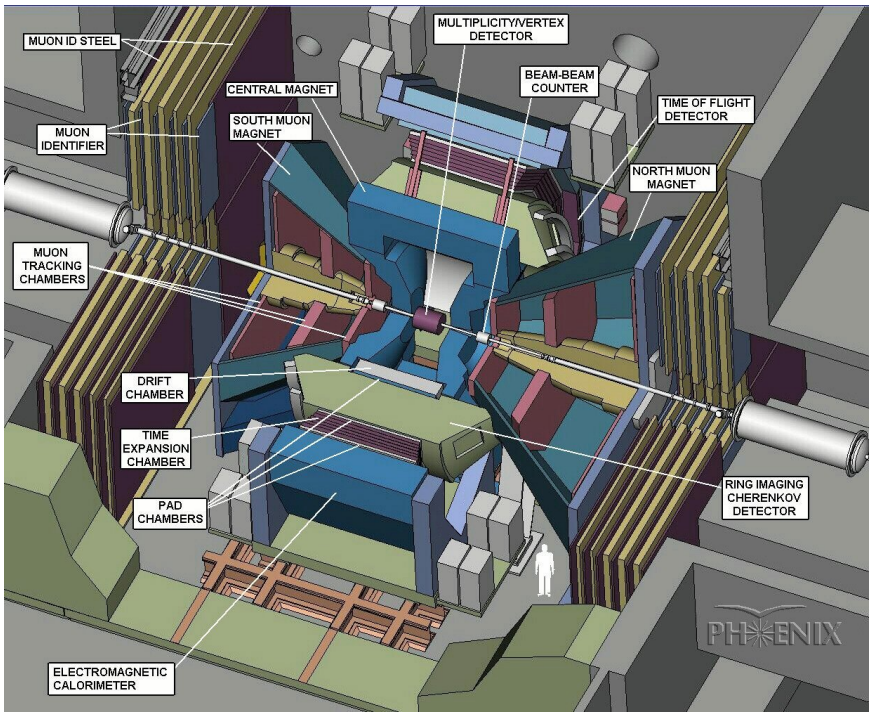

Figure 15: PHENIX experimental setup.

3.9 STAR

3.9.1 Physical overview

Solenoidal **T**racker **a**t **R**HIC.
This experiment on RHIC at BNL aims, as its primary target, at studying the process of formation and properties of QGP [9]. It will allow us to better understand the Early Universe at the stage when symmetries are being broken and restored. [10] STAR is capable of studying Au-Au collisions at $\sqrt{s_{NN}} =$ 20 to 200 GeV per nucleon pair and proton-proton collisions up to $\sqrt{s} \simeq 500$ GeV. RHIC is also the first accelerator capable of preparing polarized proton beam, which opens new opportunity to study the spin structure of the proton. Experiment is still progress and we are getting new results from the data analysis every year.

3.9.2 Experimental setup

[2] It is a large 4π hadronic particle detector with 4m diameter and 4m long solenoidal 0.5T magnetic field volume, which surrounds the main charged particle tracking device of the setup, a TPC with 50cm inner and 200cm outer radius and 45 planes of tracking. This allows to measure particles in the pseudorapidity range $-2 \leq \eta \leq +2$ and the design is able to measure particles with momentum 60 MeV/c and more. The Silicon Vertex Tracker (SVT) consists of three layers of silicon drift detectors and it surrounds the main interaction region between 5 and 15 cm enabling one to observe the strangeness produc-

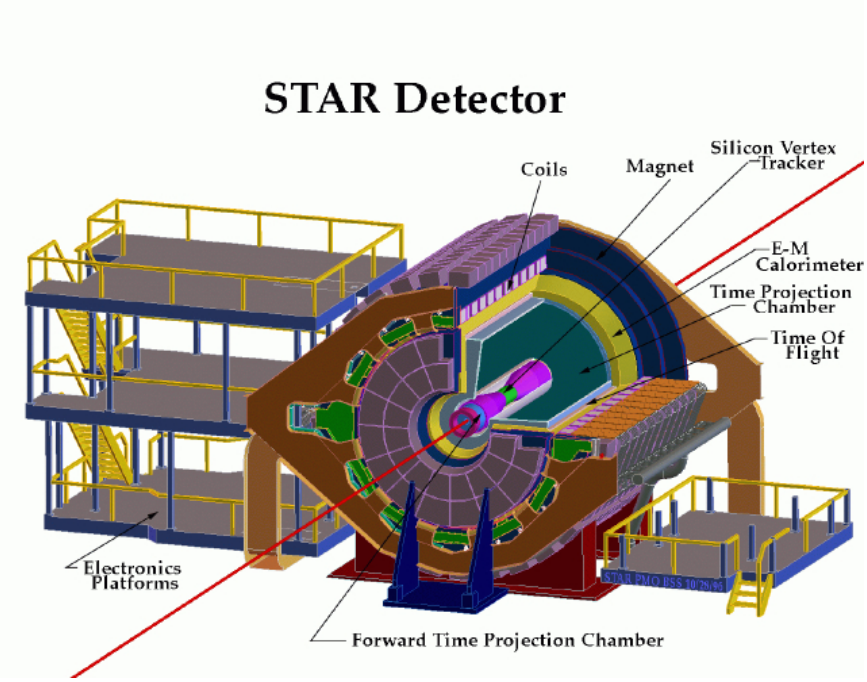

Figure 16: STAR experimental setup.

tion. The outside electromagnetic calorimeter (EMC) serves for measuring jets of particles, fluctuations and high-$p_\perp$ phenomena.

4 ALICE

4.1 Introduction

4.1.1 ALICE in LHC experimental program

High-energy physics have close connection to the evolution of the Universe, because its properties (baryon asymmetry, galaxy distribution, etc.) are believed to be connected with phase transitions which took place in the early stages of the Universe (as mentioned also in section 2.1). Reaching higher and higher energy in ultra-relativistic heavy-ion collisions let us study more and more fundamental properties of strongly interacting matter. At RHIC we were able to reach the energy of 200 GeV per nucleon. At LHC (see Appendix A), we will be able to work with 5.5 TeV per nucleon for the heaviest ions, which will allow us to extend the energy scale at which we have experimental data to compare with theoretical predictions. Targets of the whole LHC program are numerous, from "simply" studying the QGP properties in ALICE, precise measurement with b-quark studying CP-symmetry-violating processes in LHCb to search for Higgs boson in ATLAS and CMS.

4.1.2 Observables

Particle multiplicities
[11] The most fundamental observable, which will be the first to measure, is the *averaged charged-particle multiplicity per rapidity unit* $\mathrm{d}N_{ch}/\mathrm{d}y$. It fixes a global property of the medium produced in the collision. As it is related to the attained energy, it enters the calculation of most other variables.

Total transverse energy
Next important observable is the *total transverse energy per rapidity unit* at mid-rapidity. It determines the amount of the initial energy transformed into the transversally escaping particles.

Particle spectra
The yield of particle of each type is measured, because it can help in reconstructing the initial fireball state properties. As the particles are produced in the late freeze-out stage, we have the information about the particle distribution in the freeze-out and from there we can assume to the initial state properties. We have indirect probes to study the QGP phase. The spectra provide information about the freeze-out temperature, chemical potential, size parameters, elliptic flow parameters, etc.

Radial and elliptic flow
The QGP was believed to behave as an ideal gas. Based on recent experimental data, the QGP is more ideal liquid. Therefore we use hydro-dynamics for its description.
We can define the flow velocity $v(x)$ as

$$v(x) = \frac{\mathbf{P}}{P^0}$$

for every infinitesimal volume at space-time point x with 3-momentum $\mathbf{P}$ and total energy P^0. The flow describes the average momentum of particles around

space-time point x. In central collisions, we observe almost all particles emitted in the perpendicular plane to the beam axis, the fireball is spherically symmetric. Expansion of the fireball is what we call the *radial flow*. In a non-central collision (a collision with impact parameter $b \neq 0$) the fireball has an elliptic shape. During the thermalization of the fireball, it will try to re-establish equilibrium by restoring the ideal spherical shape and doing so, changing the momentum at different points of the fireball. This is what we call the *elliptical flow*. The flow is responsible for the final state particle momentum distribution.

Particle correlations
There is a big difference between heavy-ion collisions and simpler systems. We observe collective behavior of matter under extreme conditions and their large space-time extent. At high multiplicities, there are two effects leading to measurable correlations: (a) wave function quantum symmetrization (or anti-symmetrization) due to Bose-Einstein (resp. Fermi-Dirac) statistics; (b) final-state interactions between the produced particles either Coulomb or strong interactions. At lower multiplicities, we can introduce correlations to global energy-momentum ar charge conservation.

Fluctuations
Any physical quantity measured in an experiment is subject to fluctuations. The most efficient way how to extract additional information about a system created in heavy-ion collision is to study fluctuations on event-by-event basis, where specific observable is measured on event-by-event basis as well. The fluctuations measurement provide us with equivalent data as two-particle correlation in the same acceptance region.

Jets
In the collision, there are color charged partons (quarks and gluons) at high energy-momentum, which then undergo series of deexcitations and branchings, which degrade the energy and momentum of their daughter products. At the final state, a shower of colorless hadrons is present instead of one color-charged particle with very high energy. The final state analysis can be done in different ways depending on what we are interested in. It can be partitioned into clusters of hadrons originating from the same initial particle. This is what we call a '*jet*' and it facilitates track reconstruction of the primary hard partons of the initial state of the collision. Jet is defined by its size and each of the jets is assigned transverse energy $E_\perp$, pseudorapidity η and azimuthal angle ϕ. This clustering leads to track reconstruction and determination of the properties of the mother-parton of each jet.

Direct photons
Photons created in the early collision do not interact strongly with the medium, the fireball becomes for them transparent, so that they provide a good probe of the early collision stage. They are produced in parton-parton scattering. Yet we have to suppress photons from the decay $\pi^0 \longrightarrow \gamma\gamma$,which are similar to the ones of interest and when the fireball expands, there are more photons emitted from quark-quark collisions inside the fireball. There are more photon-producing processes during the expansion and freeze-out, but these photons are sufficiently lower on energy scale than the direct ones, so we can subtract them easily from the photon spectrum.

Dileptons
Another important tool for measuring the temperature and dynamical properties of the matter produced in relativistic heavy ion collision are lepton pairs emitted throughout the evolution of the system. As in the case of photons, leptons do not interact strongly with the fireball. Therefore leptons created in hard nucleon-nucleon collision are not affected by further evolution of the fireball. Of course there are lepton pairs produced in other stages of the system, from thermal radiation from the QGP to final state meson decays.

Heavy-quark and quarkonium production
Charm and bottom quark provide sensitive probe of the collision dynamics. These two quarks are produced in primary collisions and live long enough to be possibly affected by the plasma during the thermalization phase. High temperature of the system may allow also thermal production of heavy quark-antiquark pairs and to form quarkonium states. Typical observables of interest are total production rates, transverse momentum distribution and kinematical correlations between heavy quark and antiquark. Next step is to compare results from p-p, p-A and A-A collisions.

4.2 Experiment Design

4.2.1 Overview

The experiment is well described in [12] but some decisions and development was made since that time. Individual parts of the system are well described in Technical Design Reports ([13] for ITS, for instance). More actual state is briefly introduced in [11], which I will introduce as the most recent data. Of course changes and little optimization is being made every day. (For actual information and last changes see [14].)

ALICE is a general purpose experiment, whose detectors (see figure 17) mea-

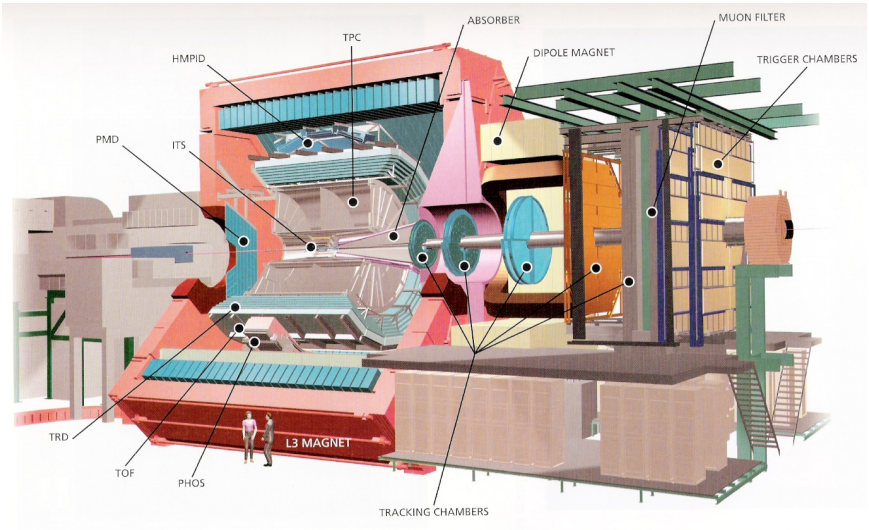

Figure 17: ALICE detectors overview.

sure and identify mid-rapidity hadrons, leptons and photons produced in the

collision. It is able to detect particles from quite low $p_\perp$ ($\simeq$ 100 MeV/c) to quite high ($\simeq$ 100 GeV/c) at high charged particle multiplicities (about 8000 charged particles per rapidity unit) Muons are detected in a dedicated spectrometer covering large-rapidity region $-4.0 < \eta < -2.4$. Hadrons, electrons and photons are detected in central rapidity region $-0.9 < \eta < 0.9$ by a complex system of detectors with a moderate ($\sim$0.5T) magnetic field present. Tracking relies on a set of high granularity detectors: Inner Tracking System (ITS) composed of six layers of silicon detectors; large volume Time-Projection Chamber (TPC) and high granularity Transition-Radiation Detector (TRD). Particle identification in the central region is done by measuring the energy loss in the tracking detectors, transition radiation in the TRD, Time-Of-Flight (TOF) with high-resolution array, Cherenkov radiation with High-Momentum Particle Identification Detector (HMPID) and photons with crystal PHOton Spectrometer (PHOS). Other detectors (Forward Multiplicity Detector (FMD), V0 and T0 detectors, Photon Multiplicity Detector (PMD) and Zero Degree Calorimeter (ZDC) for measuring spectator nucleons in heavy ion collisions) located at large rapidity regions complete the central detection system to characterize the event and to provide the interaction trigger.

4.2.2 Inner Tracking System (ITS)

The Inner Tracking System consist of six cylindrical layers of silicon detectors, located at radii $r = 4, 7, 15, 24, 39$ and 44 cm. It covers rapidity range of $|\eta| < 0.9$ for all vertices in the interaction diamond (about 10.6 cm along the beam direction) and is optimized for high impact-parameter resolution and efficient track finding. The outermost layer is determined by the necessity to match tracks from the TPC and the innermost by dimension of the beam pipe (3 cm). The innermost layer has extended rapidity coverage $|\eta| < 1.98$ to provide ,together with the FMD, continuous rapidity coverage for measuring charged particle multiplicity.
Because of high particle density (up to 80 cm^{-2}), silicon pixel detectors (SPD) have been chosen for the innermost two layers and silicon drift detectors (SDD) for the two central layers. The outer layers consist of two double-sided silicon micro-strip detectors (SSD). SDDs and SSDs will have analog readout for particle identification via $\mathrm{d}E/\mathrm{d}x$ measurement in non-relativistic region. This will give the ITS a capability as a low-$p_\perp$ particle spectrometer.

Individual detector modules will be bonded to carbon-fibre supports, called ladders. On those, there will be readout chips installed, microcables going along the ladders to the DAQ system for further data analysis, and cooling pipes, because silicon detectors are sensitive to temperature changes. Each of the layers consists of different number of ladders with different dimensions (as evident from the figure 18).

4.2.3 Time-Projection Chamber (TPC)

The TPC (figure 19) is the main tracking detector inside the ALICE central barrel and together with other barrel detectors provides charged-particle momentum measurement with good two-track separation capability, particle identification and vertex determination.

The ALICE TPC is designed for particle track density as none before, about

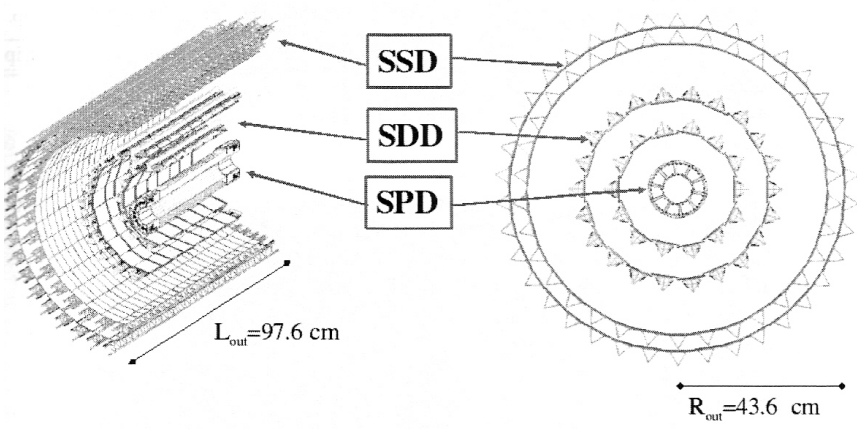

Figure 18: ITS scheme.

20000 charged primary and secondary tracks in the acceptance. Therefore special effort had to be made in the R&D activities of TPC design and tracking software optimization. Proper gas filling of the TPC was decided to be Ne/CO_2 (90%/10%) ude to its low diffusion and low radiation length and therefore low multiple scattering. It is very sensitive to temperature changes, so thermal stability of $\Delta T \leq 0.1$ K has to be assured in the whole volume over the running period. Finally, tracking efficiency $\geq 90\%$ has been reached.

4.2.4 Transition-Radiation Detector (TRD)

Main goal of TRD is the electron identification in the central barrel with momenta greater than 1 GeV/c, where the pion rejection capability of the TPC is no longer sufficient. Together with the ITS and TPC, it will provide electron identification to measure light and heavy vector-meson resonances and dilepton continuum in Pb-Pb and p-p collisions. Information from the TRD measurement of high-$p_\perp$ electrons can be used to determine open charm and open beauty production in the collisions. The detector, in order to cover the same rapidity region $|0.9| \leq \eta$, consists of six layers. For the adequate azimuthal resolution, there are 18 sectors, and 5-fold segmentation along the z-axis. In total 540 detector modules. Each module is filled with Xe/CO_2 (85%/15%) gas mixture which is the radiator, and Multi-Wire Proportional Chamber (MWPC) used for the detection and readout electronics.

4.2.5 Time-Of-Flight detector (TOF)

The TOF detector of ALICE is a large area array that covers the central rapidity region ($|\eta| \leq 0.9$) for Particle IDentification (PID) in the intermediate momentum region (from 0.2 to 2.5 GeV/c) Since the majority of produced particles is emitted in this range, the performance of such detector is of crucial importance for the experiment. The measurement of particles and their identification will provide data from which can be used to probe the nature and dynamical evolution of the system produced in ultra-relativistic heavy-ion collision at LHC energies. The TOF will provide event-by-event particle identification of large

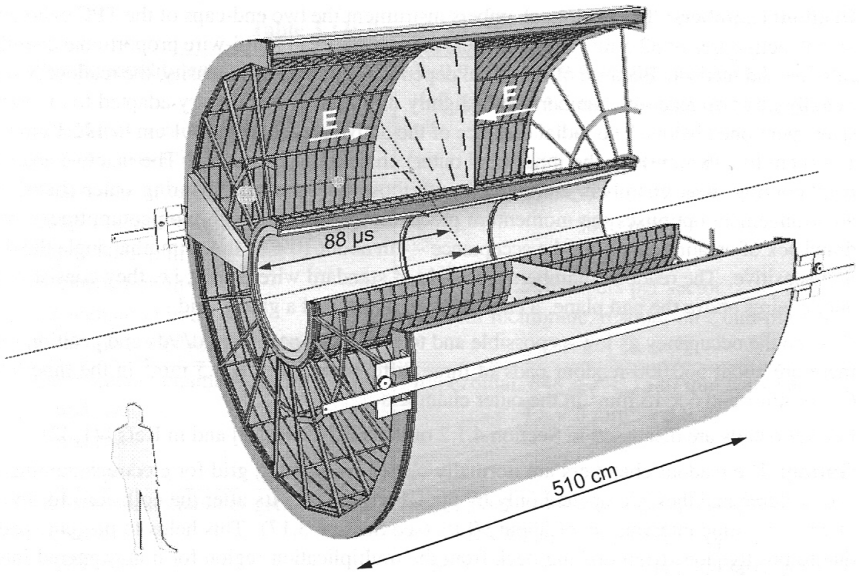

Figure 19: TPC layout.

samples of pions, kaons and protons. The R&D program has shown that the best solution for TOF detector is the Multi-gap Resistive-Plate Chamber (MRPC). Similarly to the TRD, the detector is of cylindrical design with modular structure corresponding to 18 sectors in the azimuthal angle and to 5 segments in the longitudinal coordinate along the beam axis. It can be found from 370 cm to 399 cm from the beam axis.

4.2.6 High-Momentum Particle Identification Detector (HMPID)

The HMPID is dedicated to inclusive measurement of identified hadrons for $p_\perp > 1$ GeV/c. It is designed as single-arm array with an acceptance of 5% of the central barrel phase-space (see figure 20). This detector will enhance the overall ALICE particle identification capability by enabling PID beyond the momentum interval attainable through energy loss (ITS and TPC) and time-of-flight (TOF) measurements. The detector was optimized to extend the useful range for π/K and K/p discrimination, on track-by-track basis, up to 3 GeV/c and 5GeV/c respectively. The detector is based on proximity-focusing Ring Imaging Cherenkov (RICH) counters and consists of seven modules of about 1.5×1.5 m^2 each. It will be mounted in two o'clock position of the space frame (fig. 20). As the radiator, the low chromaticity C_6F_{14} (perfluorohexane) liquid will be used. Cherenkov photons will be detected by MWPC.

4.2.7 PHOton Spectrometer (PHOS)

It is high resolution electromagnetic spectrometer which will detect electromagnetic particles in a limited acceptance range at central rapidity and provide photon identification and neutral mesons identification through their two-

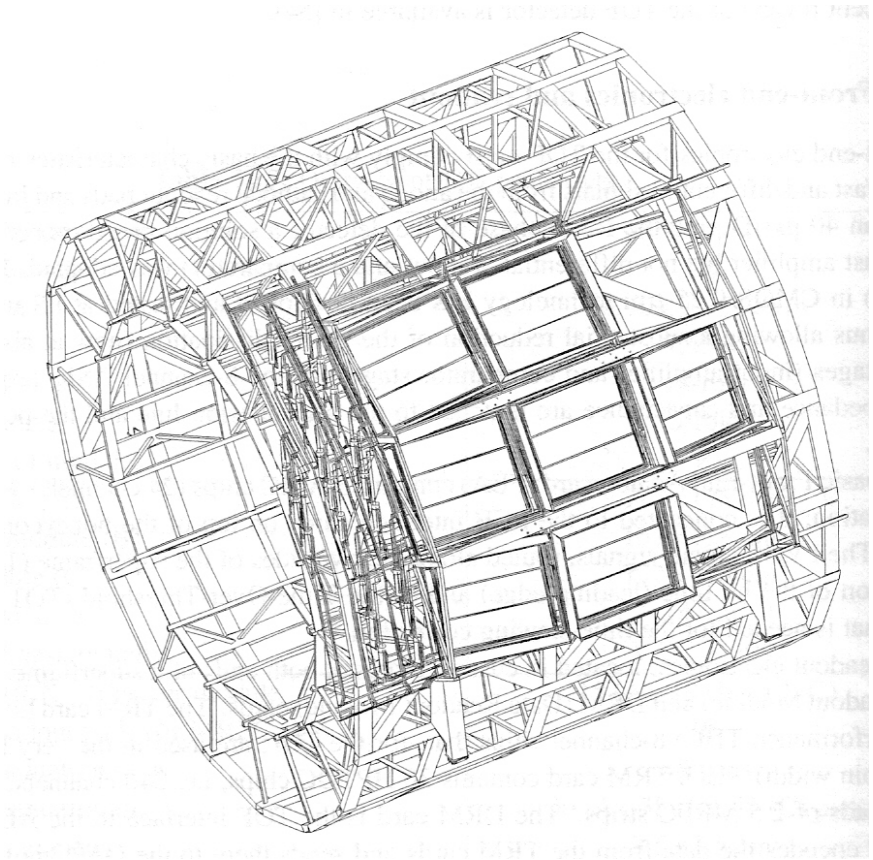

Figure 20: HMPID position in the ALICE setup.

photon decay channel. The PHOS consists of highly segmented ElectroMagnetic CAlorimeter (EMCA) and Charged Particle Veto (CPV) detector. It is situated at a distance of 460 cm from the interaction point on the bottom of the ALICE. It will cover pseudorapidity range of $-0.12 < \eta < 0.12$ and 100° in azimuthal angle. The CPV has charged-particle detection efficiency better than 99%, which is very important for charged particle exclusion from EMCA data. The EMCA is modular detector which uses lead-tungstate crystals ($PbWO_4$, also referred to as PWO) as a scintillator and Avalanche Photo-Diode (APD) as signal amplifier. To increase the light yield (by a factor of ~ 3) of the PWO crystals, the EMCA modules will be operated at a temperature of $-25\,^{\circ}\mathrm{C}$ established with precision of $\sim 0.3\,^{\circ}\mathrm{C}$.

4.2.8 Forward muon spectrometer

Hard, penetrating probes, such as heavy-quarkonia sattes, are essential tool for probing the early stage of heavy ion collisions. At LHC, energy densities are high enough to melt the $\Upsilon(1s)$ will be reached. This depends on open charm and open beauty multiplicity, so their measurement is of crucial importance. The complete spectrum of heavy quark vector mesons (J/ψ, ψ', Υ, Υ'', Υ') as

well as the Φ meson will be measured in the $\mu^+\mu^-$ decay channel in the forward muon spectrometer. It covers the polar angular range $2^\circ - 9^\circ$. It consists of a passive absorber to absorb hadrons and photons, high-granularity tracking system of 10 detection planes, large dipole magnet and passive muon filter wall followed by four planes of trigger chambers.

4.2.9 Zero-Degree Calorimeter (ZDC)

The most directly related to the collision geometry observable is the impact parameter. It can be measured by determining the number of participants and/or spectator nucleons in a collision. This is done in the ZDC, which measures the energy carried in the forward direction (at zero degree relative to the beam axis). The ZDC will be placed at 116 m from the interaction point (IP), where the distance between the beam pipes (~ 8 cm) allows detector insertion. As the magnetic elements of the LHC beam line deflects spectator protons, two distinct detectors will be used, one for protons (outside the beam line, where positive particles are deflected) and another for spectator neutrons (in the beam axis of ALICE).

4.2.10 Photon Multiplicity Detector (PMD)

The PMD is a pre-shower detector that measures the multiplicity and the spatial distribution of photons on an event-by-event basis in the forward region of ALICE. It addresses physical issues related to event-by-event fluctuations and provide estimates of transverse electromagnetic energy. PMD consists of two identical planes with thick lead converter in between them. The first plane is used for charged particle vetoing and the second behind the Pb converter is the pre-shower plane, which registers hits from both photons and charged hadrons. The PMD is located at 360 cm from the IP, on the opposite side of the muon spectrometer, covering region of $2.3 \leq \eta \leq 3.5$.

4.2.11 Forward Multiplicity Detector (FMD)

The main functionality of silicon strip Forward Multiplicity Detector is to provide charged-particle multiplicity information in the pseudo-rapidity range $-3.4 < \eta < -1.7$ and $1.7 < \eta < 5.1$. The FMD will allow the study of multiplicity fluctuations on event-by-event basis and for flow analysis in the considered pseudorapidity range. Together with ITS,the FMD will provide early charged particle multiplicity distributions for all collision types in pseudorapidity range $-3.4 < \eta < 5.1$. The detector consists of 51200 silicon strip channels distributed over 5 ring counters each divided to 20 or 40 sectors in azimuthal angle.

4.2.12 T0 and V0 detectors

These relatively small detectors are designed to provide trigger signals for other detectors. V0 consists of two round plates located asymmetrically on each side of the IP. One (V0L) at 355 cm opposite of the muon spectrometer and the other (V0R) at 90 cm from the IP just before the front absorber of the muon spectrometer. It will have the function of centrality detector and validation signal for the muon trigger to filter background in p-p mode. The T0 consists of two arrays of Cherenkov counters. Like the V0, T0 consists of two parts which

are located asymmetrically to the IP, one at 70 cm from the nominal vertex on the muon spectrometer side and the other is grouped with V0, FMD and PMD at 350 cm on the other side. The T0 detector have a few functions in the ALICE: provides timing T0 signal for the TOF with 50 ps precision; it measures vertex position (if in the desired preset range) with a precision ± 1.5 cm and provide L0 trigger; provides early "wake-up" signal to TRD, prior to L0; measure particle multiplicity and generate signal about primary vertex centrality.

4.2.13 Data AcQuisition (DAQ) system

In experiment like ALICE, there is a lot of events, which are interesting to study. They are so frequent, that the limiting factor is the performance of the DAQ system. The task of ALICE Trigger, Data AcQuisition and High-Level Trigger (HLT) (see [11]) systems is to select interesting physics events, to provide efficient access to these events for the execution of high-level trigger algorithms and finally to archive data to permanent data storage for future analysis. The raw data bandwidth from the front-end electronics is about 25GB/s, which are in parallel transferred to the DAQ system by a hundreds of optical links. Then following high level triggering, there are the Global Data Collectors (GDC), which build the events and send them (at 1.25GB/s rate) to the Transient Data Storage (TDS) and from there to the Permanent Data Storage (PDS).

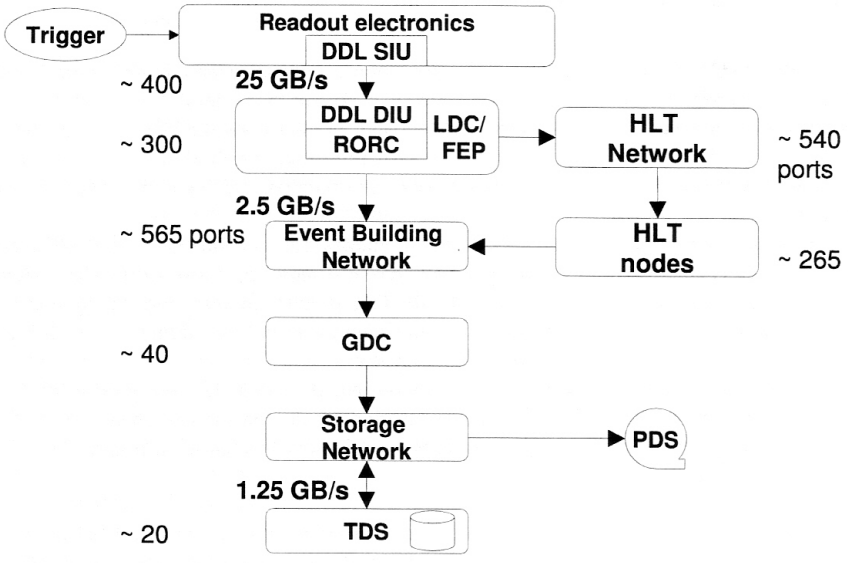

Figure 21: DAQ system scheme with data bandwidth comments.

5 Conclusion

According to present description of elementary particles, they are divided into two big groups, quarks and leptons. Each of them have specific properties and interacts differently with each other. Concentrating on the quarks and their strong interaction in heavy-ion collisions, it is believed that the matter undergoes a phase transition to completely new phase called quark-gluon plasma, where quarks and gluons are not bound in hadrons anymore. This happens at extremely high temperature (around 170 MeV) and energy density (around 1 GeV/fm). In the experiments, we can use different probes of the system (proving heavy-quark (s,c,b) pairs production in the QGP and other important variables) supporting the hypothesis of the phase transition. We are reaching higher and higher on the energy scale with new accelerators and more precise experimental data due to development of better detection techniques. At present, the experiment we are waiting for is ALICE at LHC, where we will be able to reach energy about 5.5TeV per nucleon in heavy ion collisions, which is about 30 times more than previous experiment STAR at RHIC. ALICE is a multipurpose detector, which does not concentrate on one topic, on the contrary, it tries to cover large acceptance region and respectable number of observables. First experimental data are expected in 2007. Currently, the detector is being assembled and installed to its final position.

6 Appendices

A CERN accelerator complex

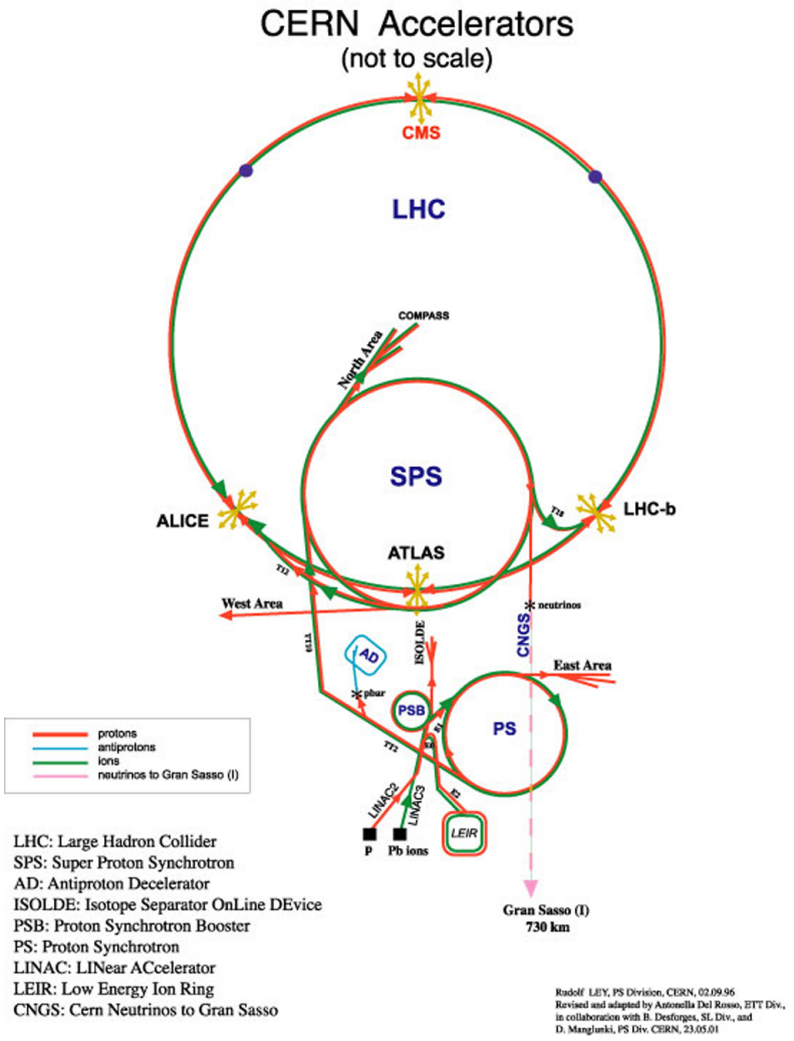

Figure 22: Nowadays accelerators at European Center for Nuclear Research - CERN (Geneva, Switzerland).

B RHIC accelerator complex

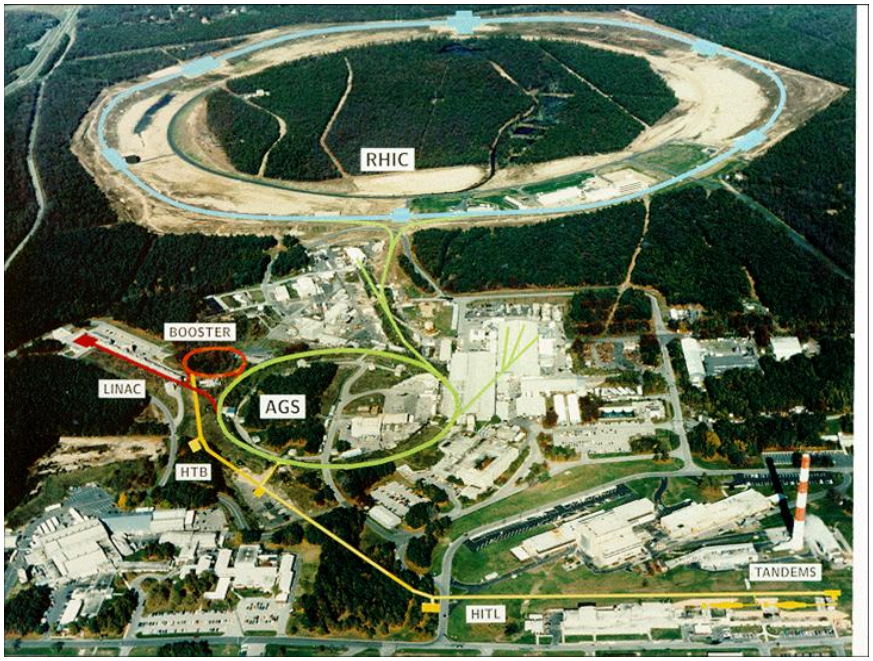

Figure 23: Photo of Brookhaven National Laboratory with its accelerator complex.

References

[1] David J. Griffiths. *Introduction to elementary particles.* John Wiley & Sons, inc., 1987.

[2] Jean Detester & Johann Rafelski. *Hadrons and Quark-Gluon Plasma.* Cambridge University Press, 2002.

[3] http://documents.cern.ch/cgi bin/setlink?base=greybook& categ=abstracts&id=NA50. *CERN document archive, NA50 abstract.* 1999.

[4] http://documents.cern.ch/cgi bin/setlink?base=greybook& categ=abstracts&id=NA60. *CERN document archive, NA60 abstract.* 2004.

[5] http://wa97.web.cern.ch/WA97. *Official WA97/NA57 webpage.* 2003.

[6] A. Dainese. *NA57 Result article presented at Quark Matter 2005, Budapest.* 2005.

[7] http://wa98.web.cern.ch/WA98. *Official WA98 experiment webpage.* 2000.

[8] http://www.phenix.bnl.gov/phenix/WWW/intro/physics/index.html. *Official PHENIX webpage.* 2006.

[9] http://www.star.bnl.gov/. *Official STAR collaboration webpage.* 2006.

[10] Kirill Filimonov. *Overview of results from the STAR experiment at RHIC, Paper LBNL-53085.* 2003.

[11] *ALICE Physics Performance Report, CERN/LHCC/2003-049 ALICE PPR Volume I.* CERN Press, 2003.

[12] *Technical proposal for A Large Ion Collider Experiment at the CERN LHC, CERN/LHCC/95-71.* CERN Press, 1995.

[13] *Technical design report of the Inner Tracking System (ITS), CERN/LHCC/99-12.* CERN Press, 1999.

[14] http://aliceinfo.cern.ch/. *Official ALICE collaboration webpage.* 2005.